OPEN MAGNETIC FIELDS AND THE SOLAR CYCLE

I: *Photospheric Sources of Open Magnetic Flux*

RANDOLPH H. LEVINE*

Harvard-Smithsonian Center for Astrophysics, Cambridge, Mass. 02138, U.S.A.

(Received 29 June; in revised form 26 November, 1981)

Abstract. Models of open magnetic structures on the Sun are presented for periods near solar minimum (CR 1626–1634) and near solar maximum (CR 1668–1678). Together with previous models of open magnetic structures during the declining phase (CR 1601–1611) these calculations provide clues to the relations between open structures, coronal holes, and active regions at different times of the solar cycle. Near solar minimum the close relation between active regions and open structures does not exist. It is suggested that near solar minimum the systematic emergence of new flux with the proper polarity imbalance to maintain open magnetic structures may occur primarily at very small spatial scales. Near solar maximum the role of active regions in maintaining open structures and coronal holes is strong, with large active regions emerging in the proper location and orientation to maintain open structures longer than typical active region lifetimes. Although the use of He I 10830 Å spectroheliograms as a coronal hole indicator is shown to be subject to significant ambiguity, the agreement between calculated open structures and coronal holes determined from He I 10830 Å spectroheliograms is very good. The rotation properties of calculated open structures near solar maximum strongly suggest two classes of features: one that rotates differentially similar to sunspots and active regions and a separate class that rotates more rigidly, as was the case for single large coronal holes during Skylab.

1. Introduction

The purpose of this paper is to explore the morphology and evolution of open magnetic fields on the Sun at various times in the solar cycle, and to suggest possible physical explanations for the similarities and differences found. Because of limitations on the observation of magnetic fields on the Sun (e.g., only line-of-sight fields are measured reliably, and then only in the photosphere or low chromosphere) the existence of open magnetic field lines in the solar atmosphere must be inferred using either spectroheliograms or theoretical extrapolations of magnetograph observations. The present work relies on both of these methods, with an emphasis on the latter.

Open magnetic fields on the Sun are important for the following reasons. First, they represent the ongoing (i.e., non-transient) path of connection between the Sun and the interplanetary medium. As such, they determine the flow geometry of the solar wind as well as the sources of the wind on the Sun. Another reason for the significance of open field regions is that they are closely related to the large-scale structure of the solar magnetic field. Further, the apparently systematic nature of the large-scale solar magnetic field suggests a close connection with the solar dynamo. Although the opening of magnetic field lines to the interplanetary medium is an *in situ* process dependent on the

* Present address: Atmospheric and Environmental Research, Inc., 840 Memorial Drive, Cambridge, Mass. 02139, U.S.A.

Solar Physics **79** (1982) 203–230. 0038–0938/82/0792–0203$04.20.

specific local plasma and field properties, the most important single aspect of the magnetic field in this context is its coronal geometry, which is influenced most strongly by the large-scale structure of the field in the photosphere.

Some open magnetic field structures are coincident with the location of coronal holes. The concept of a coronal hole is an observational one (rather than a physical one), and refers to a (usually large) contiguous region of the corona which is significantly deficient in coronal emission compared to its surroundings. The existence of coronal holes is usually inferred by the use of spectroheliograms (e.g., X-ray, He II 304 Å, He I 10830 Å), but coronal holes are also detectable at the limb using a coronagraph sensitive to white-light or the coronal green line. Because the definition of a coronal hole is an observational one, it is important to maintain the distinction between coronal holes and open magnetic field regions. Coronal holes are usually identified because of their relatively large size or long lifetime, or both. However, the physical conditions implied for coronal holes (i.e., lower temperature and density, along with solar wind flow) are also present in some smaller, shorter-lived regions of open field lines. Conversely, there are apparently some large, long-lived open field structures whose physical conditions do not result in an identifiable coronal hole even though they are solar wind sources (Nolte *et al.*, 1977; Sheeley and Harvey, 1978, 1981).

The need for a distinction between coronal holes and open magnetic regions is least important during the declining phase of the solar cycle, which happens to correspond to the period of the most concentrated study of coronal holes to date (the Skylab period). Because of observations taken at that time, coronal holes are recognized as large-scale and important features of the solar atmosphere, the connection between coronal holes and high speed solar wind streams is firmly established, the rotation properties of large trans-equatorial coronal holes is known to be much more uniform in latitude than the rotation of the Sun as a whole, and the importance of active regions in contributing magnetic flux to coronal holes is known. Many of these findings are summarized in the monograph edited by Zirker (1977).

The present work extends previous work on coronal holes by analyzing coronal magnetic field models for time periods near solar minimum (approximately 18 March 1975 to 17 November 1975) and during the rising phase of the solar cycle (approximately 6 May 1978 to 2 March 1979). In the analysis which follows these calculations are compared with He I 10830 Å observations (available in synoptic format for only the later of the two periods analyzed) and with the location and evolution of active regions. In a separate analysis (in preparation) the model field calculations will be compared with interplanetary phenomena.

The major findings to be described below can be summarized as follows. During the rising phase of the solar cycle the initial appearance and subsequent evolution of open magnetic structures (as defined by potential magnetic field models) are even more closely related to the evolution of active regions than was true during the declining phase of the solar cycle. Further, at this time (rising phase) many open magnetic structures exist simultaneously within the same interplanetary magnetic polarity sector, with only the largest and oldest open field regions apparently becoming identifiable as coronal holes.

During this period He I 10830 Å radiation is not always a straightforward indicator of open magnetic structures on the Sun, and there is significant evolution of open structures due to the increasing level of magnetic activity and to the continual emergence of active regions. The rotation properties of open structures during this period show evidence of two distinct classes, on of which rotates with latitude in a manner similar to the Newton and Nunn (1951) relation for the differential rotation of long-lived sunspots and one of which rotates more nearly like the rigid rotation of large coronal holes (Timothy *et al.*, 1975).

Near solar minimum there are no direct indicators of coronal holes available in an appropriate format for this study. However, open magnetic structures, even those which are large and long-lived, are not always closely related to active regions, in contrast to the Skylab period. That is, open structures commonly appear, evolve, and disappear without the parallel appearance and evolution of active regions. In fact, new active regions often disrupt rather than promote the evolution of open structures in the models. It is suggested that near solar minimum the evolution of open magnetic structures is often due to a significant contribution of smaller-scale magnetic flux (e.g., ephemeral active regions) and that the physical conditions in the low coronal portion of open magnetic structures at such times may be different as a result of this.

2. Method of Analysis

This study uses models of the magnetic field in the solar corona which are based on the observed line-of-sight magnetic field in the solar photosphere and on the assumption of no electric currents in the corona. A brief description of these potential field models is given below. For a full discussion of the method and its more recent applications, see Altschuler and Newkirk (1969), Schatten *et al.* (1969), Altschuler *et al.* (1977), Adams and Pneuman (1976), and Levine (1977a, b). The most recent improvement of this technique, the use of a non-spherical source surface (Levine *et al.*, 1982) is not used in the present work.

We assume that the corona is current-free so that for $R_\odot \leq r \leq R_s$ the magnetic field B can be derived from a scalar potential of the form

$$V = R_\odot \sum_{n=0}^{N} \sum_{m=0}^{n} \left(\frac{R_\odot}{r}\right)^{n+1} P_n^m(\theta)\,(g_n^m \cos m\phi + h_n^m \sin m\phi) +$$

$$+ R_s \sum_{n=1}^{N} \sum_{m=0}^{n} \left(\frac{r}{R_s}\right)^{n} P_n^m(\theta)\,(\bar{g}_n^m \cos m\phi + \bar{h}_n^m \sin m\phi)\,, \qquad (1)$$

where r, θ, and ϕ are the usual spherical coordinates and the $P_n^m(\theta)$ are associated Legendre functions. The (constant) radius R_s is the position of a spherical 'source surface' whose purpose is to simulate the effect of the coronal plasma in opening field

lines. This is accomplished by requiring the surface $r = R_s$ to be an equipotential. For such a spherical source surface as outer boundary one obtains $V = 0$ at $r = R_s$ by setting

$$(\bar{g}_n^m, \bar{h}_n^m) = -\left(\frac{R_\odot}{R_s}\right)^{n+2} (g_n^m, h_n^m) \tag{2}$$

in (1). The value of R_s is then the only free parameter in the model solution.

Observations provide values of the line of sight field B_l^{obs} at $r = R_\odot$. The above harmonic expansion yields an algebraic expression for the line of sight field $B_l = B_r \sin(\theta + \beta) + B_\theta \cos(\theta + \beta)$, where $\mathbf{B} = -\nabla V$ is obtained from Equation (1) and β is the average solar B-angle during the time of the magnetic observations (i.e., β is the heliographic latitude of the observer). By requiring that the integral of $[B_l^{\text{obs}} - (B_r \sin(\theta + \beta) + B_\theta \cos(\theta + \beta))]^2$ over the photosphere be a minimum with respect to variation of the coefficients g_n^m and h_n^m, a set of simultaneous linear equations for the coefficients can be obtained. If N is the largest principal index of the coefficients g_n^m and h_n^m to be calculated, there are $(N + 1)^2$ equations and $(N + 1)^2$ unknowns, forming a $(N + 1)^2 \times (N + 1)^2$ matrix problem. However, symmetry properties of the harmonic functions decouple the equations into blocks of $N - m + 1$ simultaneous equations, reducing the largest number of independent equations which must be solved at one time to $N + 1$ (Altschuler *et al.*, 1977). For all the models used in this study a value of $N = 25$ was chosen.

The observations used in this study were made at Kitt Peak National Observatory and assembled into synoptic maps of B_l^{obs} (and of He I 10830 Å intensity for the period during the rising part of the solar cycle) by Dr J. Harvey. The synoptic maps of both B_l^{obs} and I_{10830} are constructed by averaging each suitable daily full disk observation onto a Carrington coordinate system. Each point of a daily observation is weighted by a factor $\sin^4(\phi - \phi_0)$ where ϕ_0 is the Carrington longitude of the central meridian on that day. In this way, the central meridian portion of each daily full disk observation is emphasized in the synoptic maps (Levine, 1978).

Because there is diverse evidence that magnetograph observations underestimate the polar field strength (Suess *et al.*, 1977; Pneuman *et al.*, 1978; Svalgaard *et al.*, 1978; Levine *et al.*, 1982), a correction to the measured polar field strength was introduced before the models were calculated. Specifically, poleward of 70° latitude the radial magnetic field $\Delta B = \pm B_0 \hat{r} \cos^8 \theta$, with $B_0 = 11.56$ G, was added to the magnetograph data, the sign being chosen so as to reinforce the predominant polarities of the respective polar caps. Although this correction is necessary in order to model coronal structure near the poles more reliably, the particular correction we have chosen is not a unique one for this purpose. The same correction was applied to all the models calculated.

Other possible sources of uncertainty due to the magnetograph observations are discussed in Altschuler *et al.* (1977). Among these the most significant are the zero level determination and non-linear response of the magnetograph signal. The zero level is determined for each daily magnetogram by assuming that the net flux in regions away from strong flux concentrations is zero. This is clearly the source of a possible bias due

to large-scale regions of weak net polarity covering a significant fraction of one hemisphere. However, when the daily magnetograms are averaged into synoptic maps adjustments to the daily zero level are attempted in order to account for long-term trends in the average net field strength. In any case, such corrections are near the level of the statistical noise in the averaged data.

The non-linear response of the magnetograph system is a more serious source of concern. While the Kitt Peak instrument does not suffer serious non-linear saturation effects at high field strengths, changes of line profile in sunspot umbrae do introduce a non-linear effect into the signal. This is taken into account by introducing an empirically-determined correction factor to the magnetic signal at those locations where the line intensity is below a prescribed level. Because this correction is essentially limited to sunspot umbrae the correction introduced can have an important effect on both the total and net magnetic flux measured in an active region. Thus is it possible that at least some of the open magnetic fields calculated in the models are due to a flux imbalance that is an artifact of the data reduction procedures. While there is no way at present to test this possibility on an individual basis, it should be noted that the open magnetic fields in the models presented below show no significant preference for the leading or following polarity of active regions in either hemisphere. In addition, many of the calculated open fields in active regions occur in such a way as to systematically reinforce a preexisting net polarity imbalance. These factors suggest that the uncertainties introduced by the magnetograph observing and data reduction process do not significantly alter the major conclusions of this work, although individual cases of flux imbalance, and consequent open field lines, may be suspect.

Open field lines are most conveniently chosen in analytic models by starting each field line integration at the source surface. In this way, all field lines calculated are open. Integration proceeds inwards along the local direction of **B**, and a two-step Runge–Kutta method is applied to improve the accuracy and minimize error propagation. For all the models shown below, field line integration starts at the center of each cell of a grid on the source surface with 18 latitude elements and 36 longitude elements. The longitudinal dimension of each cell is the same and equal to 10°. The latitudinal dimension of each cell is 1/9 in units of $\cos\theta$. This results in a grid whose cells have equal latitudinal dimensions when projected on the plane of the sky. A similar, though finer, grid is used at the photosphere for calculation of the coefficients g_n^m and h_n^m. The photospheric grid has 60 latitude elements and 120 longitude elements.

It is important to keep in mind the known strengths and weaknesses of potential field models. This type of model has been applied in a variety of contexts in addition to the study of open magnetic field lines (e.g., coronal structure at eclipse: Schatten, 1968; Altschuler and Newkirk, 1969; Smith and Schatten, 1970; coronal currents: Levine and Altschuler, 1974; Howard *et al.*, 1980; interplanetary magnetic fields: Schatten *et al.*, 1979; Levine *et al.*, 1977; Levine, 1978; Burlaga *et al.*, 1978; radio and MHD wave propagation: Uchida *et al.*, 1973; Jackson and Levine, 1981). However, the success of these efforts has been varied. For example, the position/polarization of type III radio bursts is very well modeled, as is the basic structure of large coronal holes and of open

magnetic fields within active regions. Less successful are modeling efforts where details of coronal structure near the source surface are important. In these cases the shortcomings of the spherical source surface as an approximation to coronal conditions is apparent. While the use of non-spherical source surface overcomes many of these difficulties (Levine *et al.*, 1982), the improvement is in details of the fit to coronal structure near the source surface. In the absence of sufficiently detailed independent observations of coronal structure, as is the case in this work, the present interpretation of the coronal models in terms of the surface morphology of the Sun would not benefit significantly from the use of a non-spherical source surface. This technique would, however, be of value in studying aspects of interplanetary structure during the periods covered by the present work.

An additional problem, discovered during the development of a technique for constructing models with a non-spherical source surface, is that all potential field models tend to underestimate the extent of the boundaries of many coronal holes (Levine *et al.*, 1981), although the shape of coronal holes is well reproduced. This is apparently due to the existence of significant currents at the boundary between open and closed magnetic field lines. These currents are present due to an expected discontinuity in field strength between open and closed field regions which compensates for an opposite discontinuity in plasma pressure.

3. Models of Open Fields near Solar Minimum

Results of field line models for Carrington rotations 1626 through 1634 (approximately 18 March 1975 through 17 November 1975) are shown in Figure 1. Several rotations are missing due to incomplete data coverage. Each panel shows, in synoptic chart format, the position of open field lines for the indicated Carrington rotation. Starting points were chosen and field lines were integrated as described in Section 2. Because this type of plot is a radial projection, only the angular coordinates of each field line are plotted. Also shown for each rotation in Figure 1 is the magnetic polarity on the source surface with negative polarity regions shaded.

Especially for the period near solar minimum the choice of source surface radius must be made in the absence of independent indicators of coronal holes or open field lines which can be compared with the models. The suggestion from both theoretical and empirical studies (Zirker, 1977; Schulz *et al.*, 1978; Burlaga *et al.*, 1978; Levine *et al.*, 1982) is that at any given time the height at which field lines become open is lower over quiet photospheric regions than it is over active regions. For example, studies of larger-scale open fields (including interplanetary fields), which are generally dominated by structures rooted in quiet regions, require a source surface near $r = 1.6 R_\odot$ (Schatten *et al.*, 1969; Levine, 1977a, b; Pneuman *et al.*, 1978) while studies of large-scale closed fields over active regions often use values near $r = 2.6 R_\odot$ (Altschuler and Newkirk, 1969; Jackson and Levine, 1981). The assumption made for the purpose of the present work is that this distinction between different regions of the Sun at a given time can be extended to apply to the whole Sun at different times. Specifically, the open fields during the time

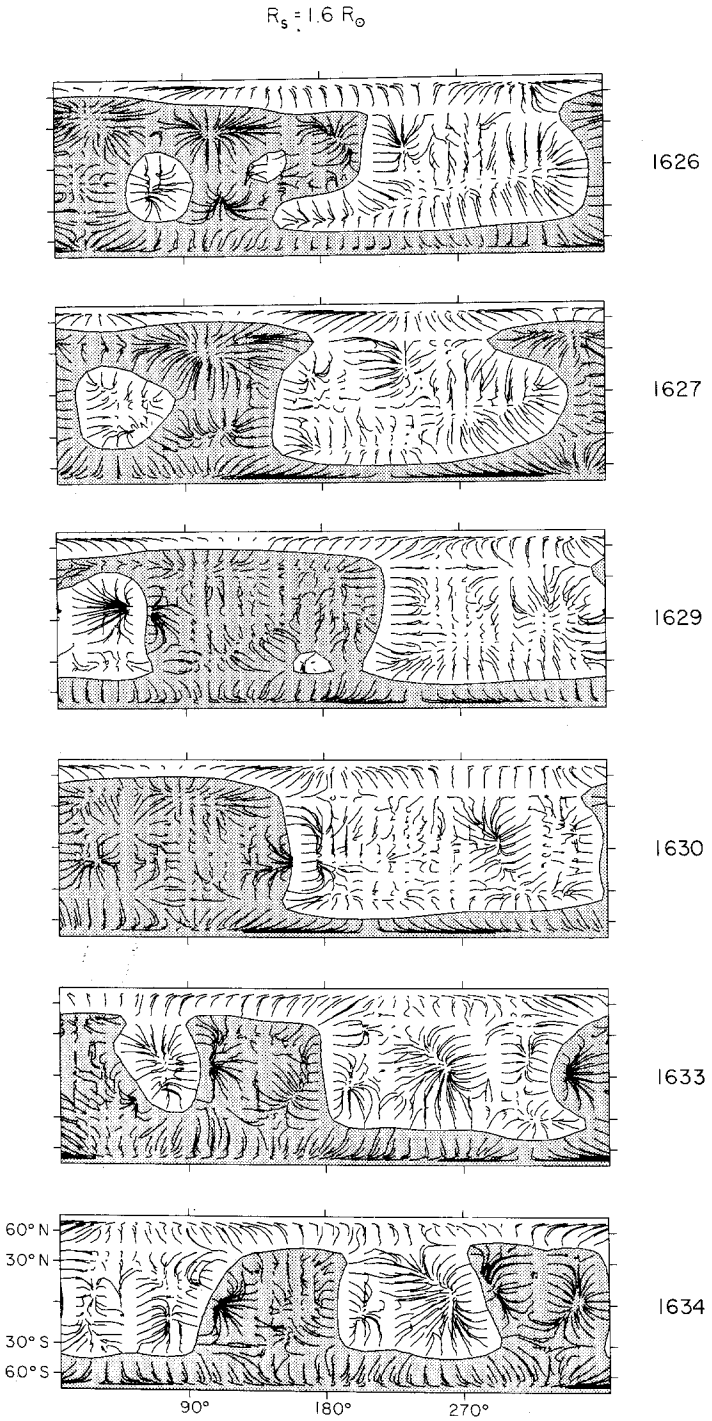

Fig. 1. Calculated open magnetic field lines for Carrington rotations 1626–1634. For these models the source surface is at a height $R_s = 1.6R_\odot$. Negative polarity regions of the source surface are shaded. Field lines lie within the range $R_\odot \leq r \leq R_s$ and are shown in projection on a synoptic chart.

of low solar activity will be modeled using a (spherical) source surface at $R_s = 1.6 R_\odot$, while open fields at times of high activity (see Section 5) will be assumed to require a higher (spherical) source surface, and $R_s = 2.6 R_\odot$ will be used. Thus, the choice of $R_s = 1.6 R_\odot$ was made for all the models in Figures 1 and 2.

Figure 2, a companion to Figure 1, shows two types of information. The individual points on Figure 2 are the photospheric ($r = R_\odot$) footpoints of the field lines shown in Figure 1. The lines are contours of B_l^{obs}, with contours for negative values shown dashed. The contour levels shown are the same for all panels of Figure 2: ± 10, ± 25, ± 50, ± 75, and ± 100 G. The growth and decay of active regions can be followed easily using the contour maps, and the evolution of footpoint regions of model open structures can be traced at the same time. Several features on Figure 2 are labelled at the edge of each panel by a letter (and sometimes a number) at both the horizontal and vertical position of the feature to aid in locating the feature on the panel. These features will be referred to in the discussion below.

The interpretation of the models displayed in Figures 1 and 2 is hindered by two unavoidable problems. First, Carrington rotations 1628, 1631, and 1632 are missing from the sequence due to lack of complete magnetograph coverage of those rotations. While there are some cases of evolutionary continuity across these gaps, there may be evolutionary sequences which begin or end during one of these gaps. A second difficulty with the interpretation of the models is the lack of continuous independent evidence for coronal hole evolution during this period. Because of this, all of the conclusions for this period must refer to the relation of model open field lines and photospheric magnetic morphology.

There are several long-lived open structures identifiable in these models (despite the data gaps, which almost certainly make it impossible to find all the long-lived structures). Two good examples of long-lived structures are the features labelled A1–A4 and B1–B4 in Figure 2. Both of these negative polarity features appear on rotation 1626 in association with active regions. This type of association is consistent with the analysis of similar models for the Skylab period. However, the subsequent evolution of these long-lived features, as represented in Figures 1 and 2, does not proceed in association with any new concentrations of magnetic flux in the photosphere. This is not the same as during the Skylab period, when long-lived model open field line structures were always maintained by new active regions systematically contributing new flux of the appropriate polarity. Another example of this apparent lack of active region involvement in the evolution of model open field regions is G1–G4. In this case the structure does not evolve in a manner consistent with what might be expected from the diffusion of magnetic flux across the solar surface, as was the case for features A and B. Instead, features G1–G4 show both growth and contraction (or perhaps this is two features; in any case, there is no apparent active region involvement).

Other examples which do involve apparent evolution in response to the dispersal of magnetic flux can also be found. Some of these are P1–P2 and R1–R2. A more problematic example is M1–M2. This evolves near two large active regions which are oriented appropriately to contribute positive flux to the model open structure. However,

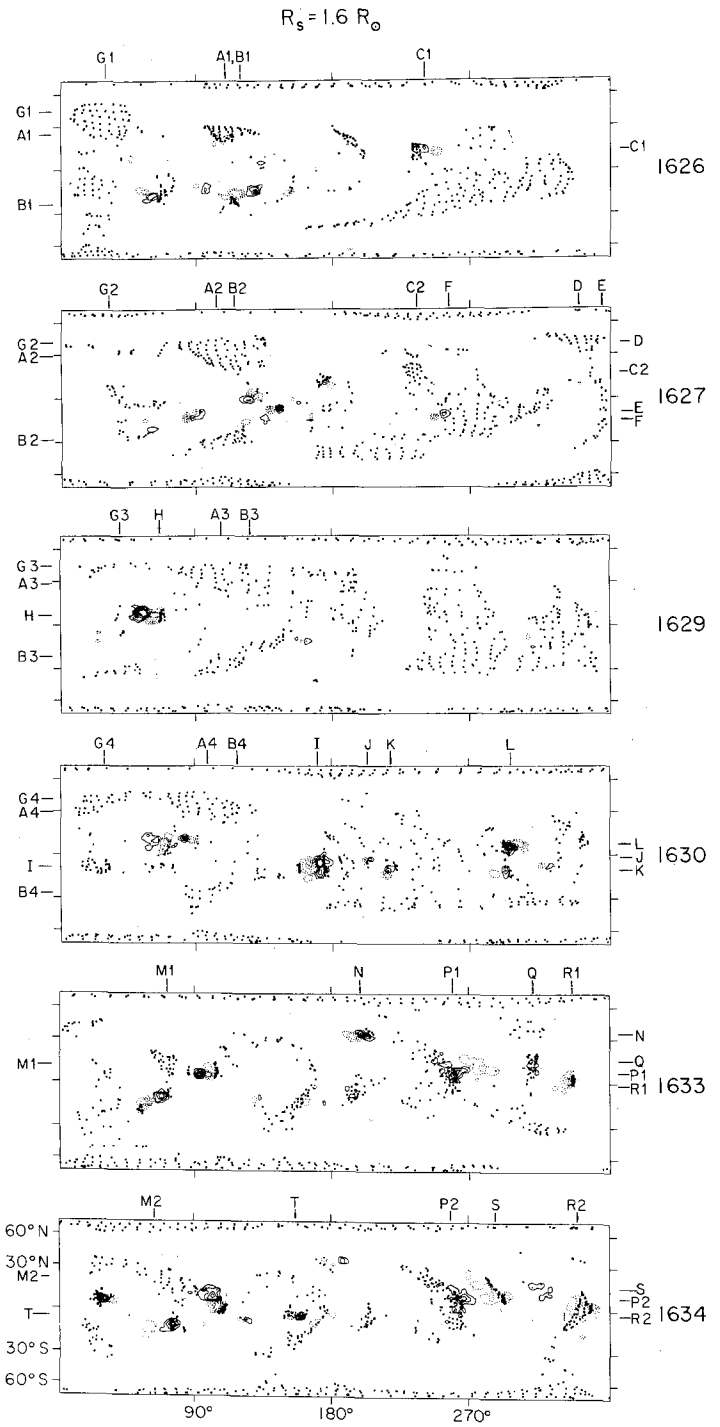

Fig. 2. Footpoints ($r = R_\odot$) of the field lines presented in Figure 1 are shown as dots. Also shown are contours of the observed line-of-sight field in the photosphere (B_l^{obs}) with contour levels of ± 10, ± 25, ± 50, ± 75, and ± 100 G. The labels outside each panel are for aid in locating features referred to in the text.

the extent of the structure becomes very great in longitude, and there are no active regions near its eastern end.

Features C1–C2 are positive polarity and clearly related to the decay of an active region present on rotation 1626. The large positive polarity feature near the same longitude on rotation 1629 may be the continuation of feature C. Both this feature and the negative polarity feature to its east on rotation 1629 are disrupted by new active regions (*J*, *K*, *L*) emerging on rotation 1630. This is completely contrary to the results of models for the Skylab period, where new active region emergence so close to an existing model open structure never caused such a large change in the structure. Moreover, the active regions which emerge on rotation 1629 cause a temporary change in the sector pattern on the source surface, from four sectors in the equatorial regions to two sectors. Less extreme examples of a new active region disrupting rather than sustaining a model open structure are features F on rotation 1627 and T on rotation 1634.

Features D and E appear first on rotation 1627 without any apparent active regions in their vicinity (although there is a small bipolar region just east of E). Because of the gap in data at rotation 1628 we cannot follow these features unambiguously. Moreover, they are very near 0° longitude which is the place where there is an unavoidable temporal discontinuity in B_l^{obs} in the models used here.

Finally, there are examples of model open field lines which appear in association with (usually new) active regions, but do not remain for even one rotation longer. Sometimes this involves the disappearance of the active region and sometimes it does not. Such features include the positive polarity portion of H on rotation 1629, N and Q on rotation 1633, and S on rotation 1634.

Two He I 10830 Å spectroheliograms taken during this period have been published by Sheeley and Harvey (1978). The 29 October 1975 spectroheliogram in their Figure 1 shows a coronal corresponding very well with feature P2 on rotation 1634. The feature R2 on rotation 1634 can be found on the 26 October 1975 observation shown in their Figure 2, although it is not pointed out by Sheeley and Harvey as a coronal hole. This same observation (26 October 1975) shows a large coronal hole whose position lies between those of features S and R2 on rotation 1634. There is no open magnetic structure in the models at this position, but one does appear at that position one rotation earlier (feature Q).

In summary, analysis of Figures 1 and 2 shows a sharp contrast with the results of a similar analysis of models for the Skylab period (Levine, 1977a, b). For the period near solar minimum, new open structures in the models are not always born in association with active regions, some are apparently never associated with active regions, and many are not maintained in association with new active regions in their vicinity. In fact, new active regions often tend to disrupt pre-existing model open magnetic structures. Although active regions clearly play an important role in relation to the open structures in the models, the close and systematic relation between active regions and open magnetic structures which existed during the Skylab period did not exist to the same degree near solar minimum.

4. He I 10830 Å Intensity as an Indicator of Coronal Holes and Open Magnetic Fields

Spectroheliograms in the He I 10830 Å absorption line have been used as an indicator of coronal holes for periods when direct observations of coronal emission were not available (Sheeley *et al.*, 1976; Sheeley and Harvey, 1978, 1981). The suitability of this line for coronal hole determinations is based on a single instance of simultaneous He II 304 Å and He I 10830 Å spectroheliograms (Harvey and Sheeley, 1977), and on the previous use of the He II 304 Å line for coronal hole studies (e.g., Bohlin and Sheeley, 1978). The difficulties in interpreting the He I 10830 Å observations have been more than offset by the ability to obtain observations from the surface of the Earth.

Coronal holes appear on He I 10830 Å spectroheliograms as regions where the chromospheric network is absent or weakened in strength. The emission from both network cell centers and network boundary elements is affected by the presence of a coronal hole. Known difficulties in locating coronal holes using He I 10830 Å observations include the presence of limb darkening in the line and the existence of 'weak' coronal holes. The former requires that coronal hole determinations be made as near disk center as possible (and makes identification of the polar coronal holes difficult). The latter are a class of coronal holes which first appeared during the rising portion of the present solar cycle. They are characterized by less contrast with the surrounding regions than in other coronal holes. The effect is not limited to the He I 10830 Å line but has been observed in soft X-rays as well (Nolte *et al.*, 1977). Such holes can be extremely difficult to locate on helium spectroheliograms, and often require the use of observations from successive days (Sheeley and Harvey, 1978).

The purpose of this section is to present several examples of apparently open magnetic structures which cannot be identified umambiguously in He I 10830 Å spectroheliograms without corroborating evidence, in this case coronal magnetic field models. These features tend to be small and/or 'weak' (in the sense described above). Similar features can be found on soft X-ray photographs (Levine, 1977a, b; Švestka *et al.*, 1977) as dark regions not large enough to be classified as coronal holes but nevertheless associated with open structures in coronal magnetic field models. During Skylab, some of these features grew into identified coronal holes.

The existence of unidentified open magnetic regions in the Helium spectroheliograms introduces an ambiguity into the correspondence between identified coronal holes and open magnetic structures in coronal field models. During the Skylab period, when most coronal holes were large and when several could be traced from beginnings as small dark X-ray or He II 304 Å features not yet called coronal holes, this ambiguity was not sufficient to hinder the interpretation of the magnetic evolution of coronal holes. During the rising portion of the solar cycle, however, the identified coronal holes themselves tend to be smaller and shorter-lived than during the declining phase of the cycle (Sheeley and Harvey, 1978). The possible existence of unidentified open magnetic regions with small scales and short lifetimes during such a period is a serious complication. The rest of this section will attempt to show, through a few clear examples, that a significant amount of

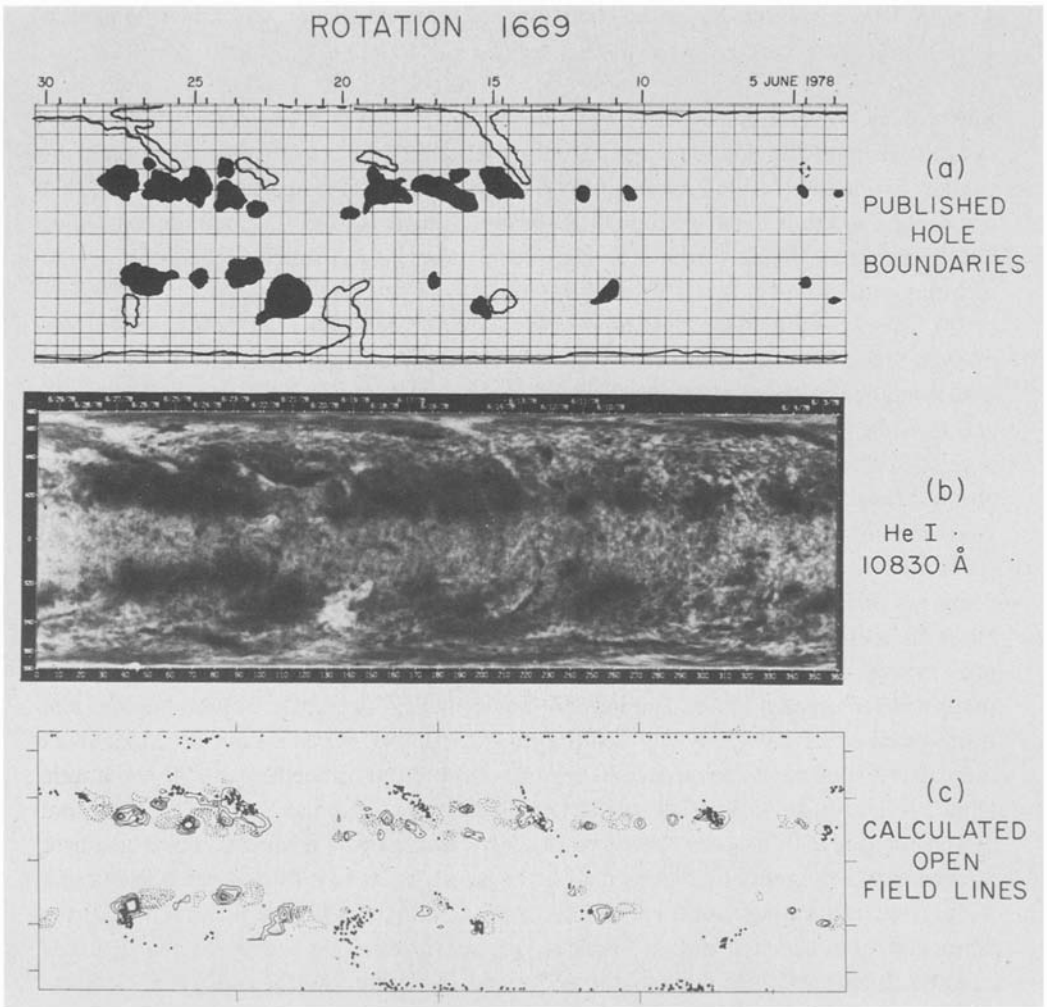

Fig. 3. Comparison of calculated open field lines and two representations of He I 10830 Å data for Carrington rotation 1669. (A): Map of coronal hole boundaries as determined by observers at Kitt Peak from daily photographic images and published in *Solar-Geophysical Data* (see text for details). (B): Synoptic chart of digital He I 10830 Å observations from Kitt Peak National Observatory. (C): Footpoints of calculated open field lines (dots) superimposed on a synoptic chart of B_l^{obs} (as in Figure 2) with contour levels of ± 25, ± 50, ± 100, ± 150, and ± 200 G.

open magnetic flux has probably not been identified using the existing procedures for analyzing He I 10830 Å spectroheliograms.

Figure 3 presents data for Carrington rotation 1669. The upper panel (A) is the map of coronal hole boundaries determined from daily He I 10830 Å spectroheliograms taken at Kitt Peak National Observatory and originally published in *Solar-Geophysical Data*. The filled areas represent plage regions and the solid outlines are the average boundary positions of regions determined to be coronal holes. Dotted outlines show short-lived or ambiguous boundaries of coronal holes. The second panel (B) is a synoptic map of

the He I 10830 Å emission for the same rotation, prepared from the digital data of daily spectroheliograms. This map is a weighted average emphasizing the near central meridian portion of each day's observation (see Section 2). Each of the coronal holes identified in panel (A) can be found on panel (B), although there is not an exact correspondence in the boundary positions because panel (A) was prepared by transfering the inferred coronal hole boundaries from a photographic image of the He I 10830 Å spectroheliogram onto a Carrington coordinate system by hand. The boundaries shown are the average over several days of the positions inferred in this way. The lower panel (C) in Figure 3 is a contour map of B_l for this rotation, with superimposed dots representing the footpoints of open field lines determined in the same way as for Figure 2, except that the source surface was taken to be at $R_s = 2.6 R_\odot$. An additional difference between (C) and the panels of Figure 2 is that the contour levels in panel (C) of Figure 3 are at ± 25, ± 50, ± 100, ± 150, and ± 200 G.

All of the eight regions identified as coronal holes in panel (A) (except for one tentative identification near longitude 340°) are represented in the model, as shown by panel (C). Notice, however, that the contrast of the coronal holes identified using the He I 10830 Å maps varies greatly. For example, the hole in the southern hemisphere near longitude 140° is quite obvious while the one near longitude 40° is of much lower contrast. In addition to the identified helium holes, there are other possible open field regions indicated by the model displayed in panel (C). Among these are a small region near a plage in the southern hemisphere at longitude 180°, small regions near longitudes 0° and 20° in the northern hemisphere, and regions in both hemispheres near longitude 300°. These last two are difficult to identify but possibly present on the He I 10830 Å synoptic chart. However, they lie in the middle of a longitude range more than 70° wide that corresponds to a six day gap in the daily spectroheliogram observations. The other three possible open field regions in the models which are not identified as coronal holes in panel (A) do correspond to regions of contrast difference in the He I 10830 Å synoptic chart that were not identified as coronal holes.

In the same format as Figure 3, Figure 4 shows information for Carrington rotation 1675. In this case the two holes connected to the north pole do not appear in the models and the hole in the northern hemisphere near longitude 90° is present but has the wrong shape. The other clear coronal holes are present in the model, though, along with many other regions of possibly open field lines. Some of these other regions that are not identified on panel (A) but which nevertheless correspond to contrast differences in panel (B) are near longitudes 60° and 180° in the northern hemisphere, and near longitudes 10° and 60° in the southern hemisphere. In addition, there is a 'bridge' in the model between the southern hemisphere hole at longitude 290° and the tentative hole in the northern hemisphere near longitude 310°. This predicted structure is obviously present in the He I 10830 Å synoptic chart. Notice that while there are two large gaps in daily spectroheliograms during this rotation, only the regions mentioned above near longitude 60° are significantly affected by these potential problems.

In addition to the features shown in Figures 3 and 4 and discussed above, there are numerous cases too subtle to present here of predicted open field regions in the models

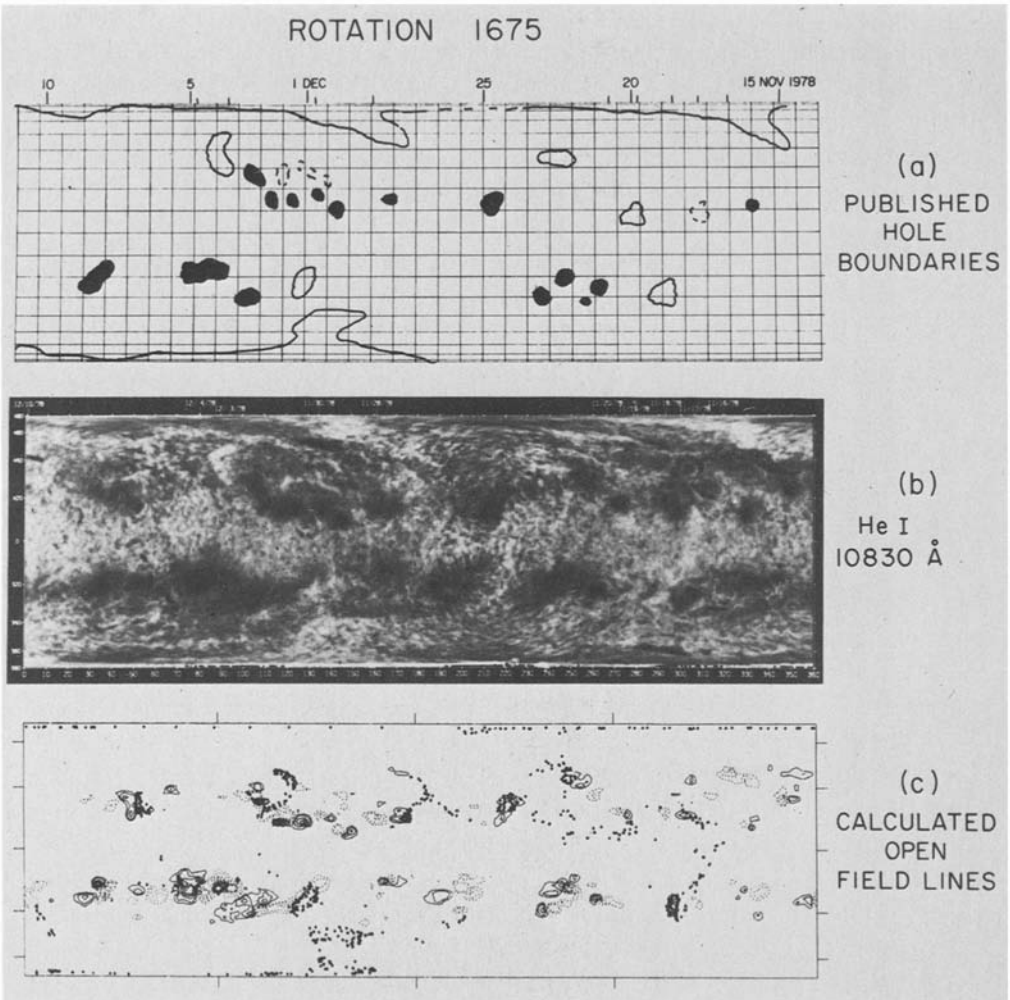

Fig. 4. Same as Figure 3 for Carrington rotation 1775.

corresponding to features which can be seen as contrast differences upon closer examination of the He I 10830 Å synoptic maps. These cases, as well as those presented in Figures 3 and 4, tend to be smaller and/or 'weaker' than the easily identified coronal holes such as those in panels (A) of Figures 3 and 4. Moreover, there are numerous open field regions in the models which are rooted partially or totally within plage regions. This was also the case during the Skylab period (Levine, 1977a, b), and these features very often can be identified as small dark features on X-ray photographs. In the present study, however, unless these active region open fields in the models extend up to or past the edge of a plage, they are very difficult to identify on the helium synoptic maps.

There is thus a potentially large amount of magnetic flux which is open to the interplanetary medium but whose footpoints are either in regions too subtle to identify

unambiguously using only He I 10830 Å spectroheliograms or in regions impossible to identify using the Helium data. The bias introduced by not identifying these areas is to over-emphasize coronal holes which are large in area and/or contrast and which are not too close to plages. Because the models indicate that a significant amount of open magnetic flux is rooted in or near plages (see Section 5), this seriously compromises the usefulness of the He I 10830 Å spectroheliograms in validating and interpreting the coronal magnetic field models.

5. Models of Open Fields near Solar Maximum

The open field line models for Carrington rotations 1668 through 1678 (approximately 6 May 1978 through 2 March 1979) are presented in Figures 5 and 6. The formats are the same as Figures 1 and 2, respectively. Parameters of the models are identical to those in Section 3 except that, as noted in Section 2, the source surface for the models shown in Figures 5 and 6 is at a height $R_s = 2.6 R_\odot$. In addition, the contour levels for B_l^{obs} in Figure 6 are at ± 25, ± 50, ± 100, ± 150, and ± 200 G.

Several recurrent and transient open field line features are marked in the margins of the panels of Figure 6 at both their latitude and longitude positions. Those labels which are underlined refer to calculated open field line regions whose photospheric positions do not correspond (within 5°) to coronal holes as noted on the maps for this period published in *Solar-Geophysical Data*, but which do correspond to regions of identifiable contrast difference on the original He I 10830 Å synoptic spectroheliograms (see Section 4 for a further discussion). Those labels which have a line through them correspond to open field regions not identified as coronal holes in *Solar-Geophysical Data* and also not verifiable as contrast differences in the original He I 10830 Å data. All the other labels (not underlined and not crossed out) are assigned to regions which correspond (within 5°) to coronal holes identified in *Solar-Geophysical Data.*

It should be noted, however, that the correspondence between the shape of the holes identified by the Kitt Peak observers (published in *Solar-Geophysical Data*) and the photospheric areas of the calculated models as shown in Figure 5 is not precise. Moreover, a comparison of the *Solar-Geophysical Data* coronal hole maps (which are produced by hand from visual inspection of up to three successive daily He I 10830 Å observations) and the He I 10830 Å synoptic spectroheliograms (which are weighted averages, typically over three to four days, of the same data in digital form) also shows significant discrepancies in boundary positions. Because of the different ways in which the published coronal hole maps and the digital synoptic averages are produced, this result is consistent with significant boundary evolution of the coronal holes over periods of a few days. It also underscores the difficulty of detecting small coronal holes, as well as growing or decaying coronal holes, in the He I 10830 Å data.

The agreement between the model open magnetic structures for Carrington rotations 1668 through 1678 and coronal holes identified using the He I 10830 Å data is summarized in Table I. (In compilling Table I polar coronal holes were not counted, but significant extensions of the polar holes were counted.) For confirmed holes identified

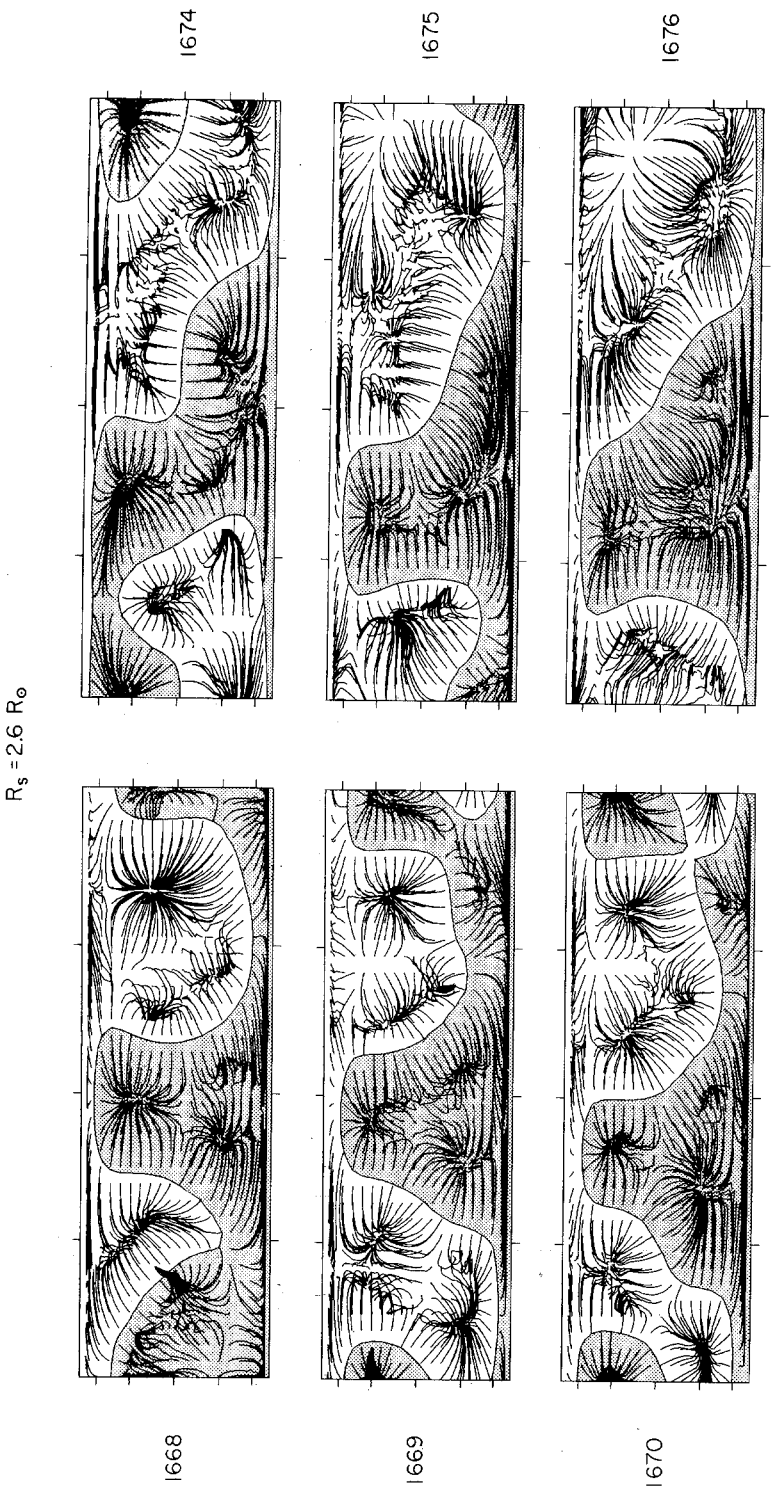
1674
1675
1676
$R_s = 2.6\ R_o$
1668
1669
1670

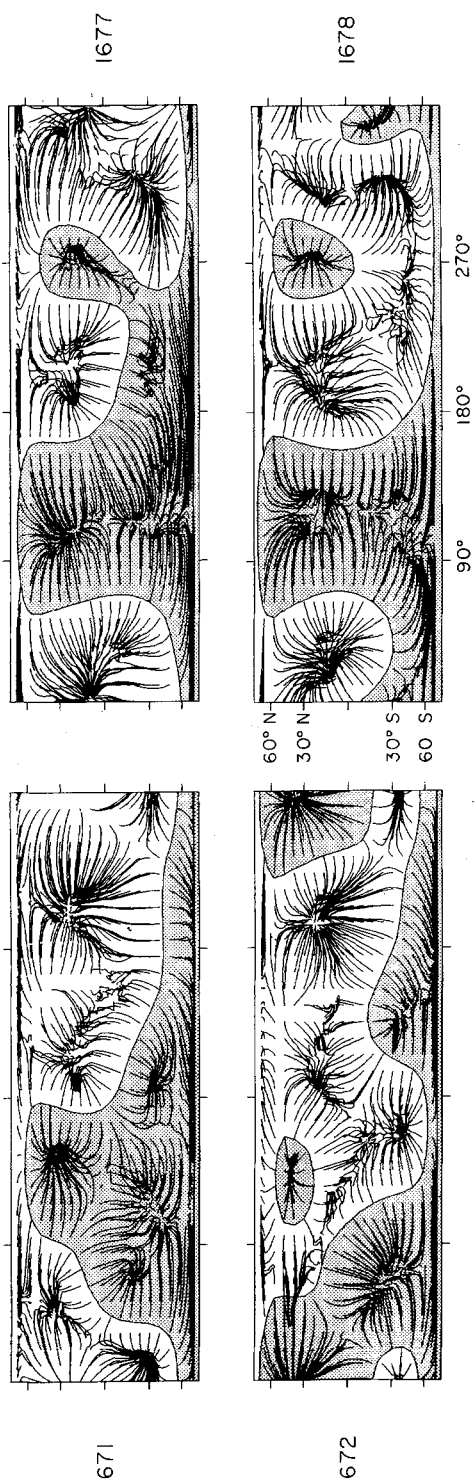

Fig. 5. Calculated open magnetic field lines for Carrington rotations 1668–1678. For these models the source surface is at a height $R_s = 2.6R_\odot$. Negative polarity regions of the source surface are shaded. Field lines lie within the range $R_\odot \leq r \leq R_s$ and are shown in projection on a synoptic chart.

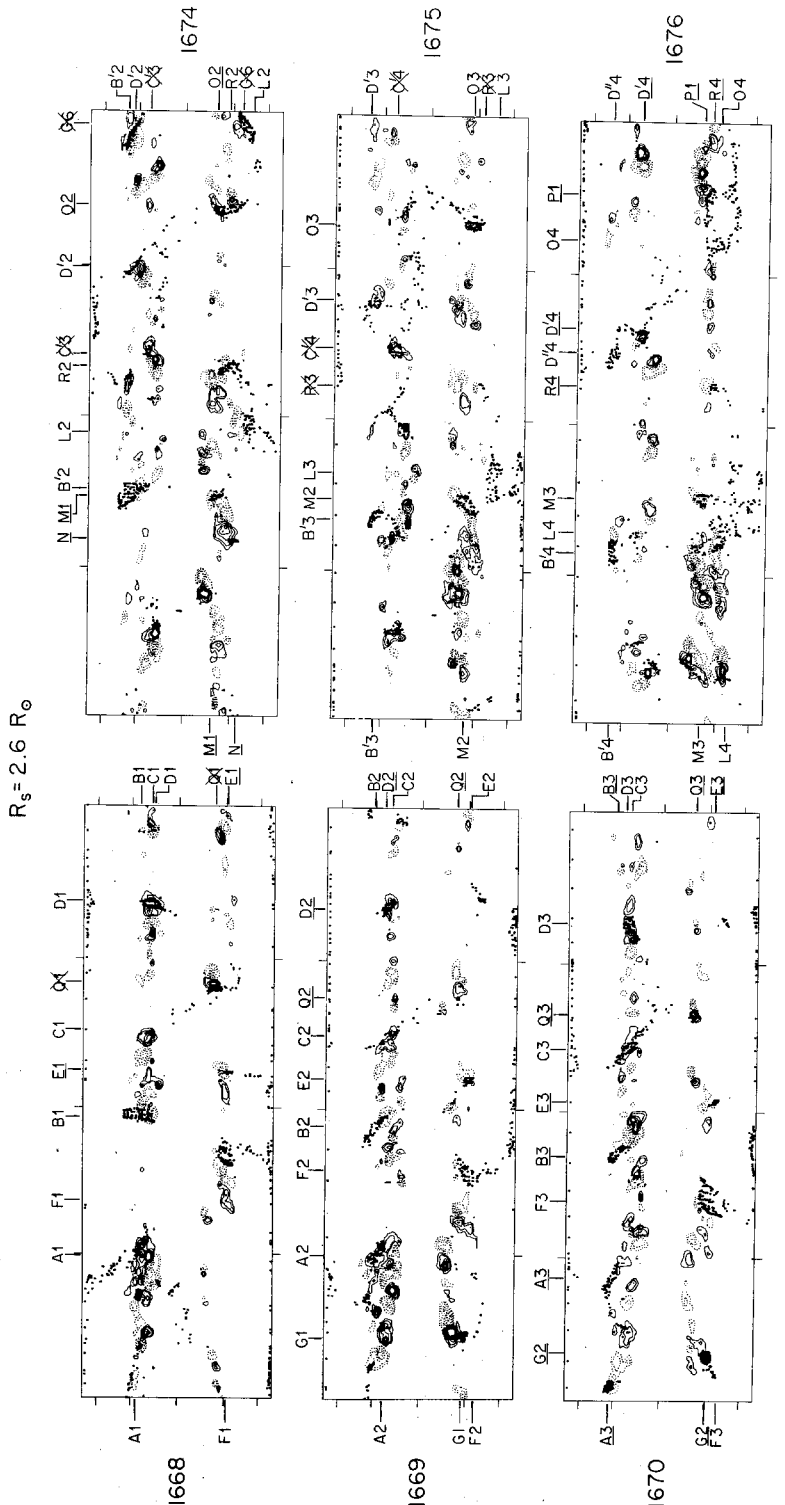
$R_s = 2.6\ R_\odot$
1668
1669
1670
1674
1675
1676

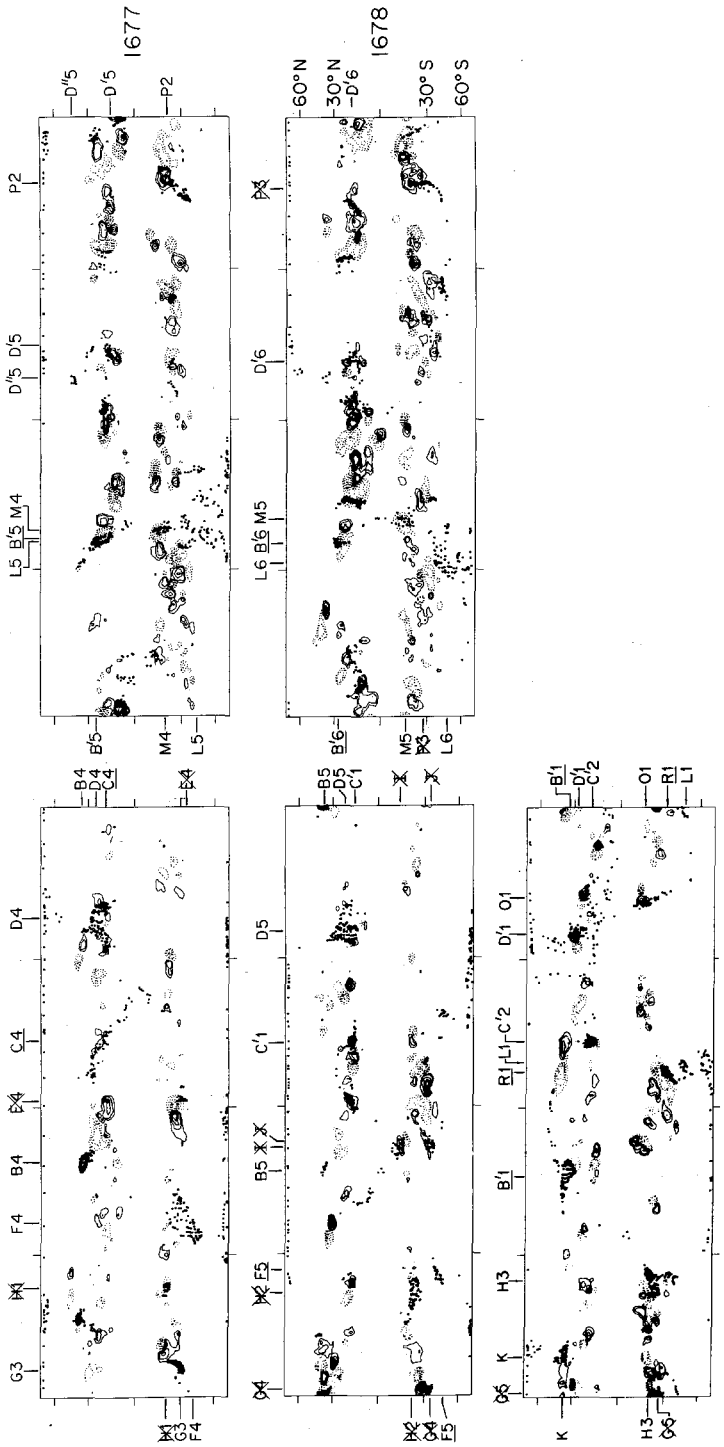

Fig. 6. Footpoints ($r = R_\odot$) of the field lines presented in Figure 5 are shown as dots. Also shown are contours of the observed line-of-sight field in the photosphere (B_l^{obs}) with contour levels of ± 25, ± 50, ± 100, ± 150, and ± 200 G. The labels outside each panel are for aid in locating features referred to in the text. Underlined labels refer to features which are identifiable as contrast differences on synoptic charts of digital He I 10830 Å observations but which were not identified as coronal holes on the maps published in *Solar-Geophysical Data* prepared by Kitt Peak observers using photographs of daily He I 10830 Å observations. Crossed out labels refer to features *not* identifiable in the He I 10830 Å data (either the *Solar-Geophysical Data* maps or the synoptic charts). All other features correspond to coronal holes identified on the maps published in *Solar-Geophysical Data* (all of which are also on the digital synoptic charts).

TABLE I

Correspondence of coronal holes and calculated open magnetic structures

Rotation	Confirmed coronal holes in *Solar-Geophysical Data*		Open magnetic structures in potential field models but not in *Solar-Geophysical Data*	
	Total	In potential field model	Total	In synoptic He I 10830 Å data
1668	7	4	6	1
1669	7	7	7	6
1670	3	1	8	6
1671	7	4	4	2
1672	5	4	10	2
1673	6	4	4	3
1674	5	4	7	3
1675	8	5	5	3
1676	5	4	9	5
1677	4	3	10	4
1678	6	6	8	3
Total	63	46	78	34

in *Solar-Geophysical Data* the number appearing in the models is 46 out of 63, or 73%. There are 78 open structures in the models not appearing on the maps published in *Solar-Geophysical Data*. However, $\frac{2}{3}$ of these are almost entirely within plage regions and would be difficult to identify using He I 10830 Å data. Even so, closer inspection of the synoptic He I 10830 Å spectroheliograms reveals that 34 of these 78 regions in the models correspond to areas of contrast difference in the spectroheliograms similar to coronal holes, as described in Section 4. Allowing for these additional regions the apparent success rate for identifying coronal holes during this period using potential field models is (46 + 34)/(63 + 34), or 82%. There remain 17 confirmed coronal holes, as identified in *Solar-Geophysical Data*, that are not present in the models during these 11 rotations.

Perhaps the most remarkable thing about the calculations presented in Figures 5 and 6 is the persistence of several open field regions over several rotations during a period of intense solar activity. For example, feature A (see Figure 6), present at the first rotation, is present on three rotations (A1–A3). Feature B, also present on the first rotation, can be seen on five rotations (B1–B5), at which time new flux appears at the same position and results in either a new feature or a continuation of the same feature for six more rotations (B′1–B′6). Feature B (including B′) thus exists during the entire period studied. Feature C is also visible for four rotations (C1–C4) and then diminishes greatly in extent but continues for four more rotations (C′1–C′4). Feature D is clearly identifiable on five rotations (D1–D5) and another feature (D′1–D′6) begins in the same position, but continues at a different rotation rate (see below). This second feature (D′) may actually bifurcate into two distinct features (labelled D′ and D″) at different

latitudes. Other examples of long-lived features and the number of rotations on which they can be found in the models are E (four rotations), F (five rotations), G (six rotations), L (five rotations), M (five rotations), and O (four rotations).

These long-lived features exhibit significantly different rotation properties. The average rotation rate of the thirteen long-lived features mentioned above (A, B, B′, C, C′, D, D′, D″, F, G, L, M, and O) lags the Carrington rate by about 10° per rotation, or almost one full day. But the range of rotation rates extends from essentially equal to the Carrington rate (features C and C′) to over 20° behind the Carrington rate (feature D″). Because these values refer to evolving and extended structures, there is no precise way to assign a rotation rate to a given feature. In determining the rotation rates quoted here the average position of the feature has been used. This is satisfactory for all but feature C, which becomes very elongated longitudinally, as if influenced by differential rotation. A similar process may have happened to features D′ and D″ which can be interpreted as differentially rotated portions of the same original structure which do not remain connected.

An especially striking example of different rotation rates is feature L and its neighbors. From near 200° longitude on rotation 1673, feature L moves to near 90° longitude on rotation 1678, or over 100° in five rotations. At the low latitude side of feature L1 is a feature labelled R1. This feature, embedded in the negative polarity portion of a large active region, stays at essentially the same longitude over a total of four rotations while feature L lags the Carrington rate substantially. On rotations 1675–1678 feature L moves completely past another structure almost stationary with respect to the Carrington rate, feature M. Whether feature M continues after the passage of feature L (rotations 1677–1678), or whether it is disrupted and an independent feature happens to appear at nearly the same position is not clear. Figure 6 is labelled assuming that feature M continues to exist during the last two rotations.

Figure 7 shows the rotation lag behind the Carrington rate in degrees per rotation vs latitude for all features labelled in Figure 6 which last more than one rotation. The latitude of each feature was determined by its average latitude at the time of its least latitudinal extent, except for feature L, which is shown over the range of latitudes near the south pole that it occupies. The range of latitudes occupied by the other features is much less than the range shown for feature L. The lag for each feature was determined by the difference in its average longitude between the first rotation on which it appears and the last rotation on which it appears. Within the uncertainty introduced by the features having finite longitudinal extent, the rotation rate for each feature is constant during its lifetime. In fact, a change in the rotation rate was used as grounds for identifying a new feature in Figure 6 (e.g., features C and C′).

Also shown on Figure 7 are two observationally determined rotation curves. One is the well-known Newton and Nunn (1951) rotation rate for long-lived sunspots. The other is the rotation rate for the large trans-equatorial coronal hole known as CH1 during the Skylab period. This rate for a single coronal hole was determined by Timothy *et al.* (1975) and is in agreement with the rotation properties of several large coronal holes as determined by Wagner (1975) from OSO-7 data. The uncertainties shown for the coronal

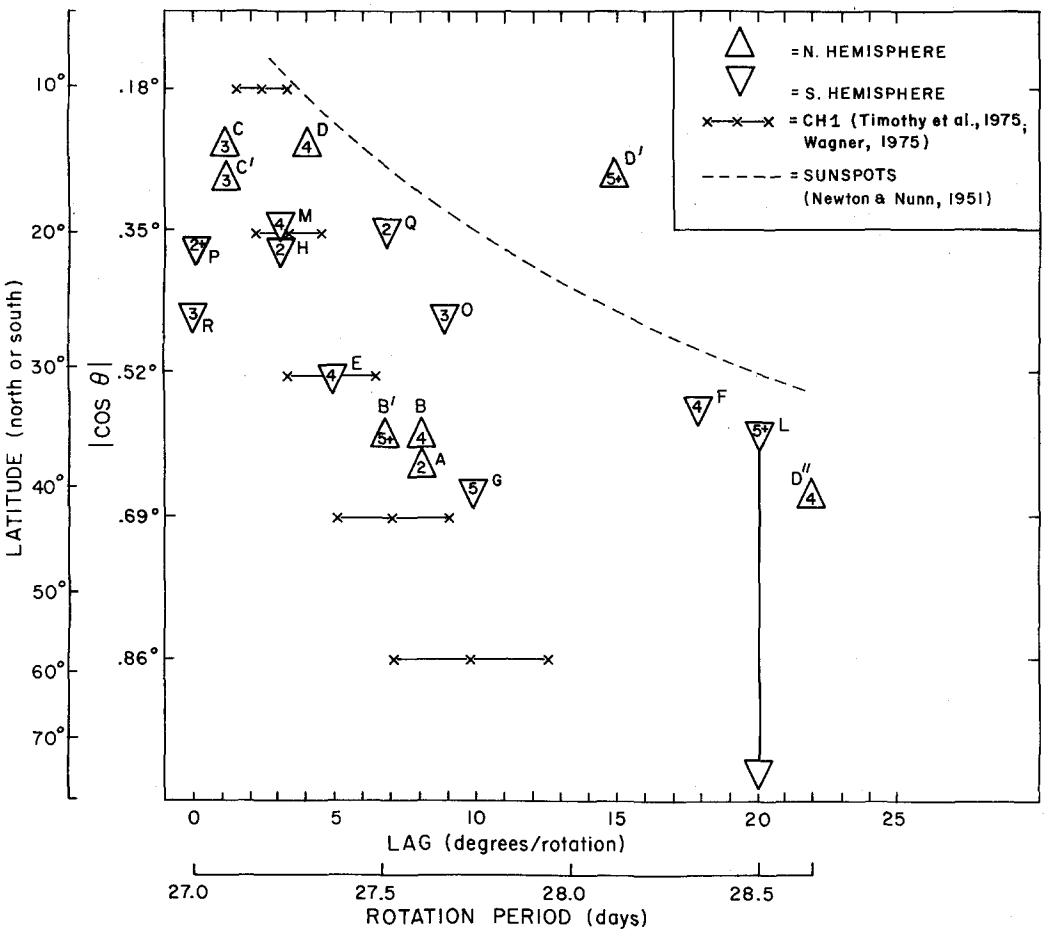

Fig. 7. Rotation of the features labelled on Figure 6 as a function of their average latitude. Northern hemisphere features are shown as triangles, Southern hemisphere features as inverted triangles. The number inside each symbol is the lifetime of the feature in rotations (i.e., the number of panels on which it appears in Figure 6 minus one). The crosses show the rotation rate for CH1 during Skylab as determined by Timothy *et al.* (1975). This also agrees with the rotation of coronal holes during the previous cycle, as determined by Wagner (1975) from OSO-7 data. The dashed curve is the rotation rate of long-lived sunspots as determined by Newton and Nunn (1951).

hole rotation curve are those given by Timothy *et al.* (1975). Krieger (1977) has argued that this curve is approximately 1σ too fast, although that does not affect the present analysis.

Although the rotation rates and latitudes of the calculated open structures (as shown in Figure 7) have a significant uncertainty that is not uniformly distributed among the features, there is a strong suggestion of two separate populations of open magnetic structure in the calculations. One class of features (hereafter, class I) rotates in a way similar to that of large coronal holes studied in the past (i.e., the curve of Timothy *et al.*, 1975), while the other (hereafter, class II) has rotation characteristics which more closely

resemble the Newton and Nunn (1951) curve for long-lived sunspots. While this distinction between two classes of calculated open structures is suggested by the data in Figure 7, it is interesting to note that the features which rotate more in accordance with the Newton and Nunn curve (class II) tend to be in only slightly better agreement with the coronal holes identified from He I 10830 Å spectroheliograms (see above) than the other group. This is true even if features at the lower latitudes, where the two groups tend to merge, are ignored. Class II features also tend to last slightly longer; the average number of rotations on which features of class I appear in Figure 6 is 4.36 while the average for class II is 4.71.

Thus it is difficult to find a significant physical distinction between these two classes of calculated open structures within the scope of the present study. This is not entirely surprising because the rotation properties of an open structure are determined by the region where it is rooted while the physical properties of the plasma (as well as the fact that the field is topologically open) are consequences of conditions in the atmosphere. The existence of two classes of open structures with possibly similar physical properties but very different rotation properties is evidence for both a differentially- and a more rigidly-rotating component of the large-scale solar magnetic field. Of course, it is possible that significant physical differences do exist between class I and class II open structures, but such differences cannot be determined from the data available here.

6. Discussion

During rotations 1626–1634 (see Section 3; Figures 1 and 2), the close association of calculated open magnetic structures in potential field models and active regions, which was established during the declining phase of the solar cycle, did not hold. The few active regions present during this period (just before solar minimum) appear to be generally unrelated to the growth or decay of calculated open structures. There are specific instances of association between open structure growth and active region emergence, but also examples of open structures which have no relation to active regions, and of open structures which persist despite obvious disruption by flux of the wrong polarity introduced by an evolving active region.

This is very curious because it is the continuing local imbalance of magnetic flux in the photosphere that leads to the appropriate topolocial conditions for open field line formation in the corona. If active regions did not always supply this imbalance near solar minimum we must ask where the flux necessary to create and maintain open structures did come from. One possible answer is that bipolar flux of a smaller scale than can be detected in the present analysis played a significant role. Ephemeral active regions (Harvey *et al.*, 1975; Martin and Harvey, 1979), for example, would not be detectable as bipolar features in the synoptic magnetograph data. However, any net flux due to a local imbalance would be present in the synoptic magnetograms, and could be reflected in the magnetic field models.

This speculation is interesting in light of the fact that perhaps half of the magnetic flux emerging through the photosphere near solar minimum (i.e., the average of flux per

feature divided by lifetime) is in the form of ephemeral active regions, as indicated by X-ray bright points (Davis *et al.*, 1977). The influence of large active regions is still significant, however, due mainly to the fact that the magnetic flux in the photosphere at any given time is dominated by larger active regions (Sheeley, 1981).

A complementary interpretation of the association of active regions with evolving open magnetic structures in the models near solar minimum is that there are two patterns present, each uncoordinated with the other insofar as open field structures are concerned. The two active region patterns would be those of the old cycle and of the new cycle, the latter being present even in 1975, some months before the actual activity minimum. It is impossible to identify old cycle magnetic flux separately from new cycle magnetic flux. However, if two patterns of active regions are present at one time it is certainly plausible that the evolution of each pattern has little to do with the other and that one pattern could disrupt consequences of the other, such as open magnetic field structures. Especially if the solar cycle is viewed as a superposition of solutions to the dynamo equations, the interference of successive cycles of the system is a distinct possibility. In making such an interpretation, we are assuming that large-scale magnetic polarity sectors in the photosphere are a fundamental aspect of the solar cycle (Levine, 1979). Such sectors are conducive to the formation of open magnetic regions in the overlying corona.

The relation between active regions, coronal holes, and open magnetic structures is very different nearer to solar maximum than it was near solar minimum. At least during rotations 1668–1678 the close relation between active regions and open magnetic structures that was apparent during Skylab existed once again. Furthermore, there is evidence that the potential field modeling technique does provide a good agreement between calculated open structures and observed coronal holes. While we cannot be as certain of this agreement as we might like (due to the ambiguity of using He I 10830 Å data as a coronal hole indicator), it is worth noting that almost all of the serious discrepancy between the calculations and inference of coronal holes from He I 10830 Å data occurs near or within plages. The helium data are not expected to provide a meaningful indication of coronal holes at such locations (Harvey and Sheeley, 1977). The existence of open field structures within active regions (Švestka *et al.*, 1977) is thus probable during this period, although it cannot be confirmed.

The major conclusions concerning the relation of calculated open magnetic field structures, active regions, and coronal holes are summarized in Table II. The conclusions from previous study of the Skylab period are listed, along with the interpretation of the same statements in relation to the data for the two time periods studied here. In general, the conclusions from the Skylab period (declining phase of the solar cycle) are also true near solar maximum, but tend to break down near solar minimum. Note, however, that independent evidence of coronal hole locations was not available for the period near solar minimum, and that the conclusions regarding the relation of open magnetic structures and active regions during that period are not sensitive to the detection of ephemeral active regions or other small-scale features (although the models are sensitive to any net flux imbalance they might cause), as noted above.

Detailed study of the rotation properties of the calculated open structures during

TABLE II

Open magnetic structures and coronal holes
(as deduced from potential field modeling)

Previous conclusions[a]	New conclusions	
Skylab period (CR 1601–1611) 5 Feb., 1973–1 March, 1974	Near solar minimum (CR 1626–1634) 18 March–17 Nov., 1975	Near solar maximum (CR 1668–1678) 6 May, 1978–2 March, 1979
All calculated open field lines are associated with either coronal holes or active regions (with very few exceptions)	Can't say – no coronal hole data.	Probably true. All calculated open structures are associated with active regions or easily identifiable remnants. The most easily identified coronal holes tend to be associated with those in remnants.
Associated coronal holes exist over only part of the lifetime of only some calculated open structures.	Can't say – no coronal hole data.	True. (But note different observational definitions of coronal holes.)
Model field lines show topological features which precede the shape of growing coronal holes by $\frac{1}{2}$ to 1 solar rotation.	Can't say. However, some structures may precede the appearance of large active regions.	True. Coronal holes are small and their boundary evolution is rapid, but a continuous sequence of calculated structures often has 1 or 2 rotations at the beginning or end without a corresponding He I 10830 Å coronal hole. Also, active regions often have associated open structures only *after* 1–2 rotations.
All calculated open structures are associated with active regions for at least part of their lifetime.	Not always true – some short-lived calculated structures remain in quiet or old plage regions. (*n.b.*, analysis not sensitive to ephemeral active regions)	Always true.
Open field lines in the models are always *born* in association with active regions.	Not always true – many open field lines appear in old plage or quiet regions. (*n.b.*, analysis not sensitive to ephemeral active regions)	Always true.
A calculated open structure is often associated with different active regions on different rotations.	This happens, but not very often. New active regions tend to disrupt previous structures more than to perpetuate them.	True. Active regions often emerge in such a way as to maintain existing open structures for several rotations.

Table II (continued)

Previous conclusions[a]	New conclusions	
Skylab period (CR 1601–1611) 5 Feb., 1973–1 March, 1974	Near solar minimum (CR 1626–1634) 18 March–17 Nov., 1975	Near solar maximum (CR 1668–1678) 6 May, 1978–2 March, 1979
All coronal holes are represented by open field line structures in the models.	Can't say – no coronal hole data.	True. But positions and/or boundaries are not always well matched. This is usually due to significant evolution within one rotation or to shortcomings of the modeling technique.

Note: Coronal holes are defined by X-ray photographs for CR 1601–1611 and by synoptic He I 10830 Å spectroheliograms for CR 1668–1678.

[a] Levine, R. H.: 1977, *Astrophys. J.* **218**, 291.

rotations 1668–1678 reveals a strong suggestion of two classes of open structures. Class I open structures rotate in a manner similar to that of CH1 during Skylab, as determined by Timothy *et al.* (1975). That is, they display very little differential rotation with latitude. Class II open structures, on the other hand, follow a rotation curve similar to that determined by Newton and Nunn (1951) for long-lived sunspots. Furthermore, there is no obvious physical distinction between class I and class II structures or their associated coronal holes, suggesting that the rotation properties of magnetic field lines rooted in the photosphere and the character of the atmosphere along the same field lines are not strongly related. That is, open field lines are created by coronal conditions and are rooted in a variety of types of photospheric locations. The present analysis suggests that this sampling of the photosphere tends to reveal two groups of magnetic field locations that can be distinguished by their rotation properties. Both differential and rigid rotation appear to be present at the same time, and coronal holes (as evidenced by calculated open structures) rotate with the more rigid pattern only if they are rooted in an appropriate photospheric location.

Similar conclusions about the presence of two rotation patterns have been made from studying the photospheric field (Wilcox *et al.*, 1970) and the green line corona (Antonucci and Svalgaard, 1974). The present analysis allows us to draw together these earlier results with the later coronal hole discoveries into a consistent picture of photospheric magnetic rotation. Antonucci and Svalgaard (1974) found that the rotation rate of the green line corona (inferred from autocorrelation functions) was slower at higher latitudes, except for periods during the declining phase of the solar cycle. From the studies of coronal holes during Skylab we now know that this more rigid rotation of the corona during the declining phase is due to the presence of large trans-equatorial coronal holes, which tend to rotate much more rigidly than the classical tracers of solar rotation.

On the other hand, the coexistence of differential and rigid rotation has been linked to either the spatial or temporal scale of features present on the Sun. For example, Antonucci and Svalgaard (1974) relate class II (i.e., differential) rotation to small spatial and temporal scale regions of activity and class I rotation to 'large scale background structures'. From the present analysis it is clear that the relation of size and lifetime to rotation properties is much more complex. The active regions which contribute to the open structures in the coronal magnetic models have a wide range of lifetimes, with no apparent systematic contribution to one rotation class or the other depending on lifetime. The influence of spatial scale is much more difficult to interpret in the present case. As for the period near solar minimum studied here (Section 3), the synoptic magnetograms do not show the smallest bipolar features on the Sun, although any local flux imbalance from such structures will appear. The identifiable features thus tend to be the larger active regions, and it is unlikely that they provide all of the magnetic flux which ends up in open structures. For the present, the most reasonable interpretation is that while the class I (i.e., rigidly rotating) features do have a (large) spatial scale associated with them, in the form of the photospheric sector pattern, there is evidence to suggest that some smaller scale magnetic features share the same rotation properties. On the other hand, the largest spatial scale which can be associated with class II rotation is that of large active regions.

During the period represented by Figure 7 the population of class I and class II open structures tended to cluster away from the region near a rotation period of 28 days. Because of this a different analysis technique (e.g., one less sensitive to individual structures) might give the impression of two separate rotation periods, one near 27.5 days and the other near 28.5 days. We cannot tell from the present analysis if this is a fundamental distinction or merely a statistical fluctuation.

If the existence of two separate rotation rates is fundamental, the likely sources of the two periods would be (a) a large-scale, more rigidly-rotating component and (b) large active regions of the new solar cycle, the latter tending to occupy the higher latitudes. It is known that there is a photospheric sector structure associated with the first of these (the large-scale, rigidly-rotating component; Scherrer *et al.*, 1977; Levine, 1979), and that active regions evolve in such a way that the sector pattern is maintained for times longer than the lifetime of an individual active region (Levine, 1977a, b). Because the calculated open structures at higher latitudes also have lifetimes longer than those of individual active regions we might expect that new cycle active regions contribute to polarity sectors there, but that the pattern rotates more slowly than the usual sector pattern near the equator. Preliminary evidence does exist for such a high latitude sector pattern, and for its slower rotation (Scherrer *et al.*, 1980). This sector pattern has two sectors and can be seen in data from both Stanford Solar Observatory and Kitt Peak.

Acknowledgements

This work was supported by U.S. Air Force contract F19628–80–C–0067 with Harvard University. Dr J. Harvey generously supplied the magnetic field and He I 10830 Å data.

References

Adams, J. and Pneuman, G. W.: 1976, *Solar Phys.* **46**, 185.
Altschuler, M. D. and Newkirk, G., Jr.: 1969, *Solar Phys.* **9**, 131.
Altschuler, M. D., Levine, R. H., Stix, M., and Harvey, J. W.: 1977, *Solar Phys.* **51**, 345.
Antonucci, E. and Svalgaard, L.: 1974, *Solar Phys.* **34**, 3.
Bohlin, J. D. and Sheeley, N. R.: 1978, *Solar Phys.* **56**, 125.
Burlaga, L. F., Behannon, K. H., Hansen, S. F., and Pneuman, G. W.: 1978, *J. Geophys. Res.* **83**, 4177.
Davis, J. M., Golub, L., and Krieger, A. S.: 1978, *Astrophys. J. Letters* **214**, L141.
Harvey, J. W. and Sheeley, N. R.: 1977, *Solar Phys.* **54**, 343.
Harvey, K. L., Martin, S. F., and Harvey, J. W.: 1975, *Solar Phys.* **40**, 87.
Howard, R., Švestka, Z., and Levine, R. H.: 1980, private communication.
Jackson, B. V. and Levine, R. H.: 1981, *Solar Phys.* **73**, 183.
Krieger, A. S.: 1977b, in J. B. Zirker (ed.), *Coronal Holes and High Speed Solar Wind Streams*, Colorado Assoc. Univ. Press, Boulder, Chapter 3.
Levine, R. H.: 1977a, *Astrophys. J.* **218**, 291.
Levine, R. H.: 1977b, in J. B. Zirker (ed.), *Coronal Holes and High Speed Solar Wind Streams*, Colorado Assoc. Univ. Press, Boulder, Chapter 4.
Levine, R. H.: 1978, *J. Geophys. Res.* **83**, 4193.
Levine, R. H.: 1979, *Solar Phys.* **62**, 277.
Levine, R. H. and Altschuler, M. D.: 1974, *Solar Phys.* **36**, 345.
Levine, R. H., Altschuler, M. D., and Harvey, J. W.: 1977, *J. Geophys. Res.* **82**, 1061.
Levine, R. H., Schulz, M., and Frazier, E. N.: 1982, *Solar Phys.* **77**, 363.
Martin, S. F. and Harvey, K. L.: 1979, *Solar Phys.* **64**, 93.
Newton, H. W. and Nunn, M. L.: 1951, *Monthly Notices Roy. Astron. Soc.* **111**, 413.
Nolte, J. T., Davis, J. M., Gerassimenko, M., Lazarus, A. J., and Sullivan, J. D.: 1977, *Geophys. Res. Letters* **4**, 291.
Pneuman, G. W., Hansen, S. F., and Hansen, R. T.: 1978, *Solar Phys.* **59**, 313.
Schatten, K. H.: 1968, *Nature* **220**, 1211.
Schatten, K. H., Wilcox, J. M., and Ness, N. F.: 1969, *Solar Phys.* **9**, 442.
Scherrer, P. H., Wilcox, J. M., Svalgaard, L., Duvall, T., Jr., Dittmer, P. H., and Gustafson, E. K.: 1977, *Solar Phys.* **54**, 355.
Scherrer, P. H., Wilcox, J. M., and Levine, R. H.: 1980, private communication.
Schulz, M., Frazier, E. N., and Boučher, D. J., Jr.: 1978, *Solar Phys.* **60**, 83.
Sheeley, N. R.: 1981, in F. Q. Orrall (ed.), *Skylab Workshop on Active Regions Monograph*, Colorado Assoc. Univ. Press, Boulder.
Sheeley, N. R. and Harvey, J. W.: 1978, *Solar Phys.* **59**, 159.
Sheeley, N. R. and Harvey, J. W.: 1981, *Solar Phys.*, in press.
Sheeley, N. R., Harvey, J. W., and Feldman, W. C.: 1976, *Solar Phys.* **49**, 271.
Smith, S. M. and Schatten, K. H.: 1970, *Nature* **226**, 1130.
Suess, S. T., Richter, A. K., Winge, C. R., and Nerney, S. F.: 1977, *Astrophys. J.* **217**, 296.
Svalgaard, L., Duvall, T. L., Jr. and Scherrer, P. H.: 1978, *Solar Phys.* **58**, 225.
Švestka, Z., Solodyna, C. V., Howard, R., and Levine, R. H.: 1977, *Solar Phys.* **55**, 359.
Timothy, A. F., Krieger, A. S., and Vaiana, G. S.: 1975, *Solar Phys.* **42**, 135.
Uchida, Y., Altschuler, M. D., and Newkirk, G. A., Jr.: 1973, *Solar Phys.* **28**, 495.
Wagner, W. J.: 1975, *Astrophys. J. Letters* **198**, L141.
Wilcox, J. M., Schatten, K. H., and Tannenbaum, A. S.: 1970, *Solar Phys.* **14**, 255.
Zirker, J. B. (ed.): 1977, *Coronal Holes and High Speed Wind Streams*, Colorado Assoc. Univ. Press, Boulder.